Resolution-Enhanced Lensless Color Shadow Imaging Microscopy Based on Large Field-of-View Submicron-Pixel Imaging Sensors

Cheng Yang
Nanjing University
Nanjing,China
njuyangcheng@163.com

Haowen Ma
Nanjing University
Nanjing,China
mahaowen2012@163.com

Xu Cao
Nanjing University
Nanjing,China
cxhenanopt@163.com

Xia Hua
Nanjing University
Nanjing,China
hxhxspark@163.com

Xiaofeng Bu
Nanjing University
Nanjing,China
buxiaofengr@163.com

Limin Zhang
Nanjing University
Nanjing,China
lmzhang@nju.edu.cn

Tao Yue
Nanjing University
Nanjing,China
yuetao@nju.edu.cn

Feng Yan
Nanjing University
Nanjing,China
fyan@nju.edu.cn

Abstract

We report a resolution-enhanced lensless color shadow imaging microscopy (RELCSIM) system based on large field-of-view (FOV) submicron-pixel imaging sensors. The physical pixel size of our custom made imaging chip is $0.95um \times 0.95um$*, and the pixel-count is 25 millions* $(5120H \times 5120V)$*. By directly recording the shadow of the samples without any postprocssing, we have realized a microscope with a half-pitch resolution of* $\sim 1um$ *and a FOV of* $\sim 25mm^2$ *simutaneously. To verify the resolution of our system, the grating samples coated on the surface of the chip are imaged. We further demonstrate the monochromatic and color shadow imaging of muscle tissue specimens with the prototype, which show the potential for applications such as diagnostic pathology.*

1. Introduction

It has been more than four hundred years since optical microscopy was invented, and various types of microscopes have been investigated for their applications in biology research and medical diagnosis [3].

Because of the limited Space-Bandwidth Product (SBP) [10] of optical systems, the conventional optical microscope suffers the inherent trade off between the high spatial resolution and large FOV [14]. Thus, it is still an extremely challenging task to produce a microscope with both submicron resolution and centimeter-level field-of-view (FOV).

In many cases, such as pathology evaluation of cancer, where both high spatial resolution and large FOV are required, the mechanical scanning scheme has to be employed to stitch a whole specimen image from hundreds of local views, sacrificing the system complexity and capability of dynamic imaging. These issues restrict the adoption of the advanced lens-based microscope for point-of-care applications, especially in resource limited settings. Besides, to eliminate the optical aberration, the complex compound lens composed of a set of optical components is required, which increases the weight and cost of conventional optical microscopes further.

To realize large SBP microscopy imaging, lensless imaging, i.e., recording the shadows or diffraction patterns of the light transmitted through a sample directly, was proposed [6]. Compared with the conventional optical microscope, lensless on-chip microscopy can not only achieve large SBP but also be portable and cost-effective. Depending on the distance between samples and the image sensors, lensless imaging can be classified into two types, i.e., the diffraction imaging [4] and the shadow imaging [6].The diffraction schemes can imaging the samples placed with a small distance from the sensor (usually 0.5mm around) by computational reconstruction from the measured diffraction patterns. Although these reconstruction based methods are flexible, the computational complexity and reconstruction accuracy limit its application in practice. Meanwhile, the shadow imaging scheme requires the samples are placed as close as possible to the surface of the imaging chip [12]. Then the light transmitting through the samples is recorded by the imaging sensor. Since the distance between the sample and the sensor is negligible, the diffraction effect can be ignored. Thus, the sharp image can be directly measured without any reconstruction or post-processing procedure. This what-you-measure-is-what-you-want character makes the system user-friendly, and thus of great potential

in real applications.

However, according to Nyquist-Shannon sampling theorem, the spatial resolution of the shadow imaging system depends on the physical size of pixels. To improve the resolution of shadow imaging microscopy, the most direct method is to reduce the pixel size. But limited by the structure of detector and manufacturing technique, the bottleneck of pixel size of existing image sensors is $\sim 1um$ [1].

In this paper, we introduce a resolution-enhanced lensless color shadow imaging microscopy (RELCSIM) system based on an imaging sensor with large FOV and submicron pixels. The main contributions of this paper are as follows: 1) We design and manufacture the submicron-pixel imaging chip (pixel size: $0.95um \times 0.95um$, $5120H \times 5120V$), and use it for shadow imaging microscopy with $\sim 1um$ half-pitch resolution and $5mm \times 5mm$ FOV. 2) Through imaging the line pairs etched on a Ag substrate, we verify the resolution of the system based on our sub-micron-pixel imaging chip. 3) We design the chip without micro lens, color filter and projective glass to realize the distance between sample and sensor of $\sim 5um$. 4) We demonstrate the full-color shadow microscopic images of tissue specimens captured by our prototype system using trichromatic ($627nm$, $530nm$ and $405nm$) sequential illumination [7]. Compared with the conventional $20\times$ objective reflective microscope, the FOV of our system is about 40 times than it in the comparable image quality.

2. Related Work

Lange *et al*. [6] demonstrated a miniaturized microfluidic shadow imaging device for studying $C.elegans$. The sample chamber, used for holding the nematodes, was placed on the monochromatic sensor directly, and the images were recorded by shadow imaging without any lenses. In this experiment, the imaging area of the camera chip is only $3.2mm \times 2.5mm$ with a resolution of 320×240 pixels. The distance between samples and the chip is $\sim 300um$. This early system is ingenious and compact, but the low-resolution ($> 10um$) limits the spread application in many cases.

Ozcan *et al*. [11] demonstrated a wide FOV imaging platform (two orders of magnitude larger ($37.25mm \times 25.70mm$) than the conventional optical microscope) for monitoring the cells on-chip, which termed as LUCAS. This system recorded the shadow image of cells onto the sensor plane to monitor and count different cell types. Because of the sensors used in the system (pixel size: $9um$) was not specifically designed for the shadow imaging, its spatial resolution is limited.

At the same time, to break through the limitations of physical pixel size and sample-to-sensor distance on resolution, Heng *et al*. [16] proposed the optofluidic microscopes (OFM) to exploit the time dimension during the imaging acquisition process. In his method, a micro-fluidic channel confined $C.elegans$ on the surface of the CMOS sensors. To improve the resolution, a tilted array of submicron metallic apertures is fabricated over the surface of the sensors and each aperture is positioned at the centre of a pixel. So the projection image of the $C.elegans$ can be sampled by the apertures as they flow inside the chamber. Finally, the resolution of the OFM is fundamentally limited by the size of the apertures and the spacing in between. By using the OFM, the resolution of the lensless and fully on-chip microscopes reached to submicron level [2]. However, there still are some challenges of OFM for wide applications, such as the changes of sample orientation and the nonuniformity of the flow rate inside the channel may deteriorate the reconstruction quality. Pang *et al*. [13] promoted the optofluidic microscope to a color-capable OFM for determining the dye concentration with varying illumination intensity.

By the aid of the pixel super-resolution methods, the spatial resolution of shadowing imaging can be improved. Zheng *et al*. [17] reported the sub-pixel resolving optofluidic microscope (SROFM) to realize a resolution of $0.75um$. The SROPM does not require an aperture array compared to the aperture-based OFM. Specifically, the samples in the micro-fluidic flow cross the surface of the sensor suffices for generating sub-pixel shifts. Through combining the obtained low resolution (LR) images from multiple sub-pixel-shift, the SROFM can reconstruct (high resolution) HR images of samples as they flow through the channel. Lee *et al*. [9] extended the SROFM to color imaging, and applied it to the observation of the blood cells for malaria diagnosis. Then, Lee *et al*. [8] demonstrated a smartphone-based microscope using ambient illumination based on the shadow imaging. To obtain the sub-pixel resolution, they performed pixel super-resolution reconstruction via capturing the images of samples at different illumination angles.

Limited by the physical pixel size and sample-to-sensor distance of commercial imaging sensors, shadow imaging suffers from the limited spatial resolution. Although series of super-resolution methods were proposed, the reconstruction quality is still unsatisfactory. So in our work, we try to solve this problem fundamentally by reducing the physical pixel size. In addition to this, the custom made chip without micro lens, color filter and projective glass can effectively reduce the distance between the sample and sensors.

3. Materials and Methods

In this section, we present the configuration of the proposed lensless shadow imaging system, including the hardware setup and detailed imaging process. In addition, the designed performance parameters of the imaging chip will be introduced and verified by experiments.

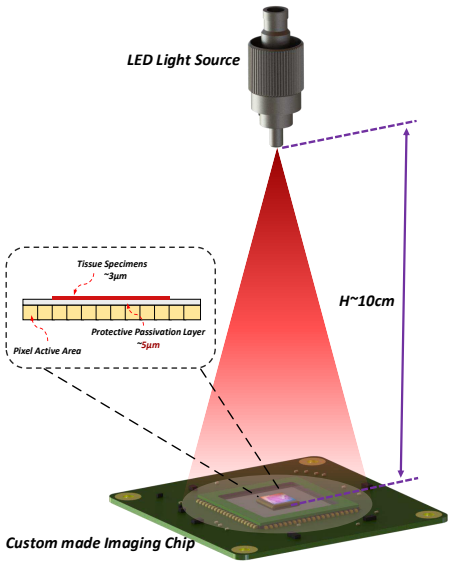

Figure 1. The schematic diagram of our RELCSIM system. The distance between the light source and the samples is $\sim 10cm$. The sample-to-sensor distance is $\sim 5um$.

3.1. System Hardware Setup

As shown in Figure 1, our lensless shadow imaging system mainly consists of three parts: a broadband light-emitting diode (LED) illumination source (LLS-627, LLS-530, LLS-405, Ocean Optics, the United States), our submicron-pixel imaging sensors (monochrome, pixel size:$0.95um \times 0.95um$, $5120H \times 5120V$), and the samples (*e.g.* tissue specimens) attached to the surface of the detector array (pathological section thickness: $3um$). To obtain the uniform illumination, the LED light source coupled to a multi-mode optical fiber (core diameter: $600um$). The distance between the light source and the samples is about $10cm$. A set of standard pathological section production procedures, which will be detailedly described in the following pages, is applied to make sure the samples adhere to the surface of the chip. Thus the sample-to-sensor distance reaches to$\sim 5um$. Since the LED light source is convenient to switchover the light-emitting modules to get red, green and blue illumination respectively, the proposed system can easily capture color microscopic images.

3.2. Imaging Process and Data Processing

The entire process of imaging and data processing of our prototype is shown in Figure 2 and described as the following stages.

Stage 1: Before imaging the samples, we capture an image pair I_{dark} (i.e., the image captured without any illumination) and I_{light} (i.e., the image under uniform illumination without samples) of each color illumination condition first. I_{dark} acts as the dark counts corresponding to each pixel, and I_{light} is used for calibrating the sensitivity of each pixel. Then, the samples are attached to the surface of our chip, and three gray-scale projection images of the samples (I^R_{sample}, I^G_{sample}, I^B_{sample}) are recorded sequentially.

Stage 2: Using the images acquired by stage 1, we next implement a flat-field correction process in the second stage. In practice, the response sensitivity and the dark count noise of each pixel is variable, leading to the fixed-pattern noise (FPN) of imaging sensors, which can be clearly seen in Figure 2.

Fortunately, the FPN can be effectively reduced by simple flat-field image processing [15],

$$I = \frac{I_{sample} - I_{dark}}{I_{light} - I_{dark}} \cdot m, \tag{1}$$

where I is the image corrected by flat-field processing, and I_{sample} denotes the real captured image of samples. m is a factor to adjust the brightness of the image, and in this paper, we set $m = mean(I_{light} - I_{dark})$.

After the flat-field correction on red, green and blue channels respectively, the color microscopic image can be easily derived by combining the three gray-scale images together.

3.3. Chip Manufacture and Performance

In order to improve the resolution of directly shadow imaging on-chip microscopy, we designed and fabricated a $0.95um$ pixel imaging chip with a kind of novel photoelectric detector based on the standard complementary metal-oxide-semiconductor transistor (CMOS) process. As shown in Figure 3(a), there are about six hundreds of imaging chips in a manufactured 8-inch silicon wafer. With the chip yield reaches to 0.1 million, the cost of a single custom made imaging chip is as low as 5 USD. Figure 3(b) briefly presents the designed layout of a single chip, including the pixel array and the peripheral circuits. Figure 3(c) exhibits our submicron-pixel imaging sensor with package. All the bonding golden wire were protected by a kind of glue, which ensures the chip can withstand the standard making process of tissue section on the surface of the chip.

The general specifications of our imaging chip are summarized in Table 1. It is important to emphasize that this paper is not focus on the device physics and structure of our novel imaging detector, but for demonstrating the application of this imaging sensor in microscopic shadow imaging. As seen in Table 1, the shape of the photosensitive area (a.k.a., the active pixel size) of a single pixel is not square, so the lateral resolution is better than the longitudinal resolution theoretically. The framerate of our prototype is slower than mature commercial products, which is limited

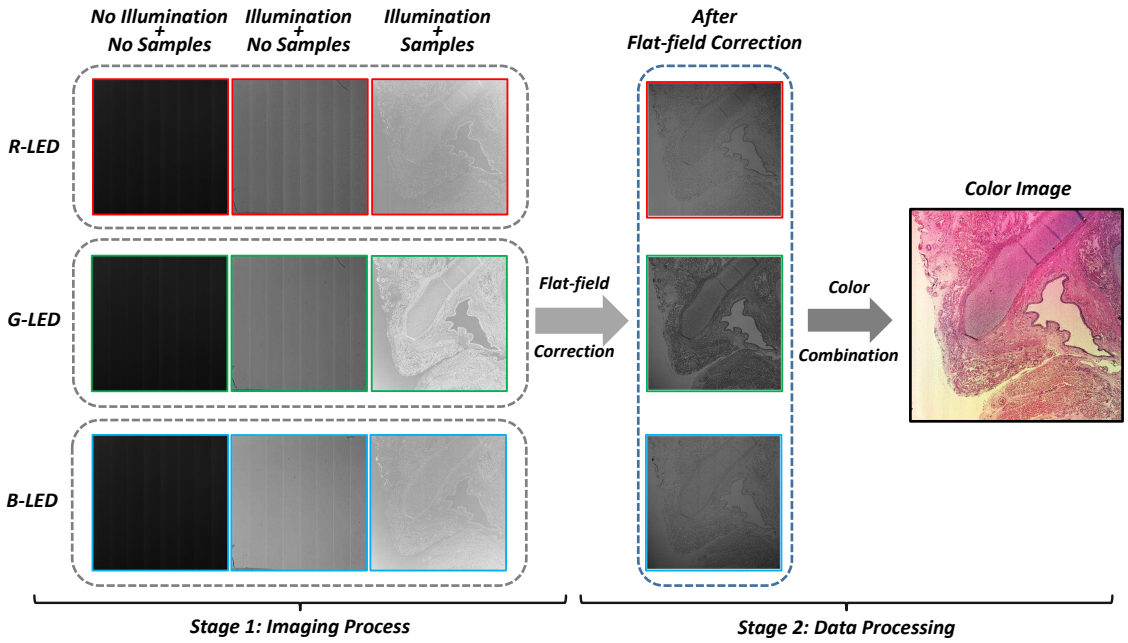

Figure 2. The flowchart of the imaging process and data processing.

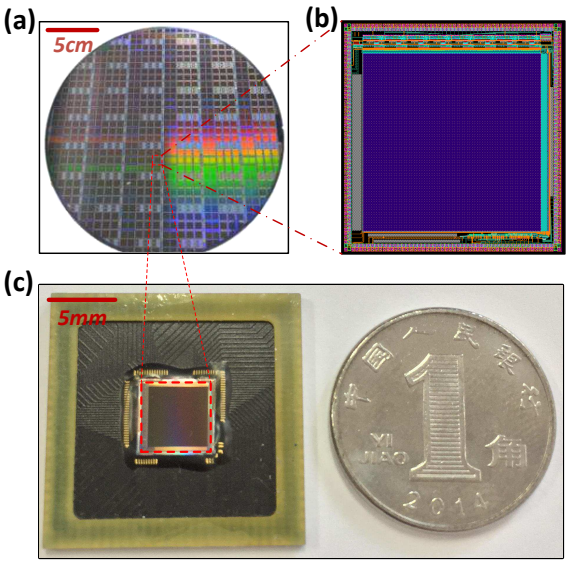

Figure 3. Illustration and picture of our custom made submicron-pixel imaging sensor. (a) Each finished 8-inch silicon wafer contains hundreds of submicron-pixel imaging sensor. (b) The designed layout of our imaging chip based on standard CMOS process. (c) The picture of our packaged chip, with which compared a dime.

Parameter	Value
Number of Active Pixels	$5120(H) \times 5120(V)$
Pixel Size	$0.95um(H) \times 0.95um(V)$
Active Pixel Size	$0.41um(H) \times 0.7um(V)$
Active Chip Size	$5mm(H) \times 5mm(V)$
Operate Mode	Monochromatic
Maximum Framerate	0.5 fps
ADC Resolution	8-bit
Package	88-pin, PLCC

Table 1. General specifications of the custom made chip.

by the speed of readout circuits of our chip. Further improving the speed and performance of the readout circuits will be on the list of our future works. It is worth noting that in order to reduce the sample-to-sensor distance, there are no micro lens or color filters on the top of the pixels in our imaging sensor. Thus, to accomplish the color imaging, we capture images with three color illuminations sequentially and combining them into a color image.

To verify the resolution of our system based on the submicron-pixel imaging sensor, some grating samples are fabricated by focused iron beam etching (FIB, Carl Zeiss Auriga, Germany) with a layer of coated Ag film on the surface of the chip as the substrate [5]. There are two directions of the sample gratings, i.e., lateral and longitudinal respectively. And the depth of the grating samples is $\sim 90nm$.

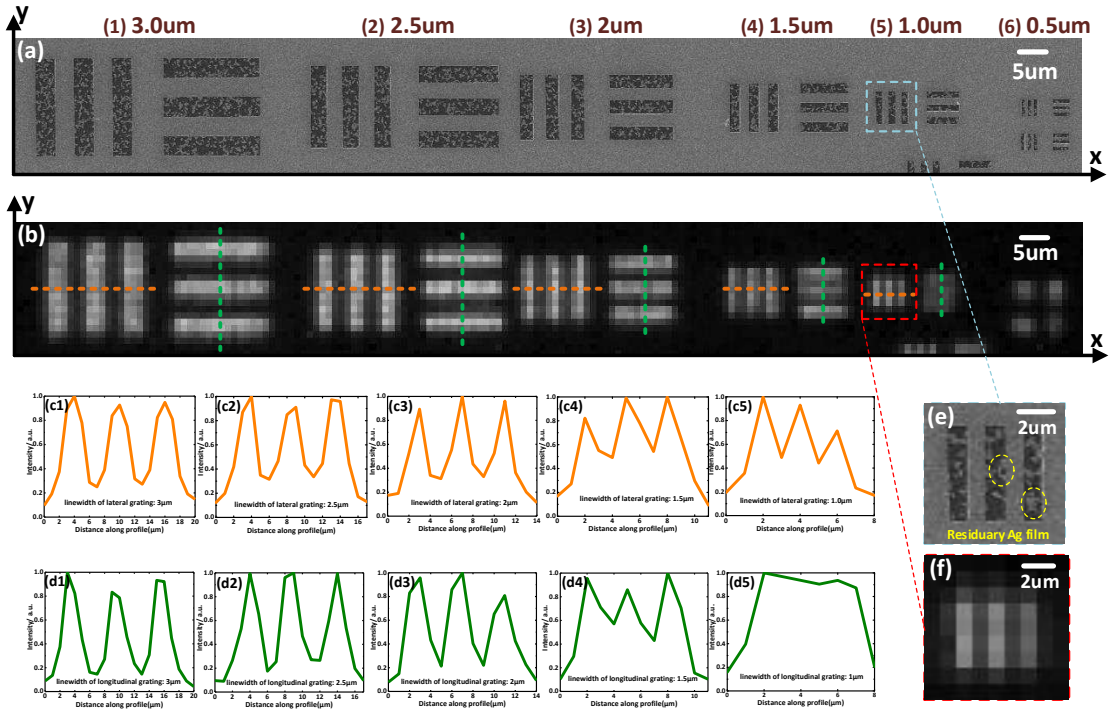

Figure 4. The experimental results of the sample gratings by our RELCSIM system. (a) The image of the grating samples acquired via $100\times$ objective microscope for comparison. (b) Sample gratings imaged by our RELCSIM system. (c1)$\sim$(c6) The line profiles along the orange dashed in the (b). (d1)$\sim$(d6) The line profiles along the green dashed in the (b). (e) The enlargement of the blue dashed boxed areas of (a), the spatial period of the grating in the image is approximately $2um$. (f) The enlargement of the red dashed boxed areas of (b). The scale bar of (a) and (b) is $5um$. The scale bar of (e) and (f) is $2um$.

Figure 4(a) shows six groups of the grating samples captured by the $100\times$ objective microscope. As shown in Figure 4(a), the linewidth of the six groups of grating samples (which is equivalent to the gaps between grating lines) varies from $3um$ to $0.5um$ with the step of approximately $0.5um$. Figure 4(b) is the image of these sample gratings obtained by our prototype. In this experiment, the central wavelength of the illumination light is $627nm$ with a bandwidth about $15nm$. Figure 4(c) and 4(d) show the line profiles along the orange dashed and green dashed to demonstrate the lateral resolution and the longitudinal resolution of our system, respectively. Figure 4(e) and 4(f) are the enlargement of the areas marked by green and red dashed boxes in Figure 4(b) and 4(c) respectively. From Figure 4(c) and 4(d), we can clearly discern the gratings from the image obtained by our custom made imaging sensor when the linewidth of the sample gratings is larger than $1um$. Furthermore, when the linewidth of the grating is just $\sim 1um$, only the lateral sample gratings can be distinguished, as shown in Figure 4(c5) and 4(d5). If the linewidth of the gratings is smaller than $1um$ (*e.g.* $\sim 0.5um$), the details of the gratings cannot be well discerned by directly shadow imaging with our sensors, since it is beyond the resolution limit of the present RELCSIM system.

It should be noted that the imaging results of sample gratings may be influenced by the residuary Ag film in the gap between grating lines as shown in the dashed round boxed area of Figure 4(e). The sample gratings is not well aligned with the edge of the pixels, leading to the crosstalk that makes the imaging results blurred. These experiment results coincide well with the theoretical prediction that the lateral resolution is better than the longitudinal resolution of our custom made imaging sensor.

4. Experiments and Results

In this section, to demonstrate the potential application of our color shadow imaging prototype for pathology evaluation, the muscle tissue specimen sample is imaged. The image of the whole sample can hardly be captured for the traditional microscope with high-magnification lens, while the proposed RELCSIM can easily achieve the FOV of $\sim 25mm^2$.

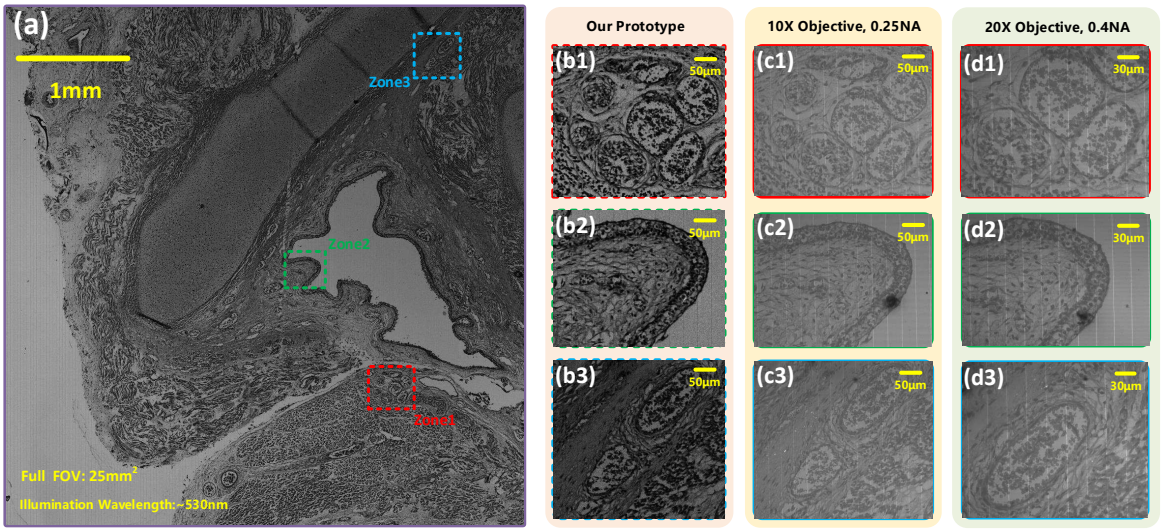

Figure 5. The monochromatic imaging results of the tissue specimens under the green LED light source. (a) The gray-scale image of the tissue specimen obtained by our prototype under an illumination wavelength of $530nm$. (b1)∼(b3) The enlargements of the dashed boxed areas of (a). (c1)∼(c3) The image with $10\times$ objective corresponding to the dashed boxed areas of (a). (d1)∼(d3) The image with $20\times$ objective corresponding to a part of the dashed boxed areas of (a).

4.1. Sample Preparation

Instead of making the tissue specimen on microslides, we use the same standard process but put the specimen on the surface of the chip. The detailed process is described as follows:

Section and Deparaffinization/Rehydration. Firstly, cutting the paraffin-embedded muscle tissue into sections of $\sim 3um$ on a microtome and floating them on the surface of warmed water. Then separating the sections gently used a metal tweezer. The most important step is to drag for the sections out of the water by our custom made imaging chip instead of the microscope slides. After that, placing the chip with the tissue sections at $60°$C for $30 \sim 60$ minutes to completely melt the paraffin. Then the chip with the tissue sections should be soaked in the xylene for deparaffinization. Next, incubating sections in 100% to 75% ethanol for 10 minutes each to rehydration. At last, washing the sections by dH_2O for at least 5 minutes.

Hematoxylin-Eosin (HE) Staining. After finished the section, deparaffinization and rehydration, the muscle tissue specimen samples is totally adhere to the surface of our imaging chip. Note that our imaging chip can work properly after the whole process above and the next HE staining. The protocol for HE staining is described as below. 1) Harris hematoxylin solution staining for 5 minutes. 2) Washing under the running water for $3 \sim 5$ minutes. 3) Differentiating in 1% acid alcohol for 5 seconds. 4) Washing under the running water for 1 minutes. 5) Staining in eosin Y solution for $30 \sim 60$ seconds. 6) Dehydrating through 75%, 85%, 95%, 100% alcohol for 5 minutes each. 7) Soaked in xylene for clear for 5 minutes. After all the procedures above, the nuclei in the tissue specimen samples would be blue and the cytoplasm would be pink or red.

The HE stained muscle tissue section (thickness: $\sim 3um$) is perfectly attached to the surface of the imaging chip directly, with only a pixel-protective passivation layer between the samples and sensor. Therefore, the sample-to-sensor distance is $\sim 5um$, which ensures the diffraction of the samples can be ignored.

4.2. Results and Discussion

The gray-scale image of the dense sample (the muscle tissue specimen) captured by our lensless shadow imaging prototype under an illumination wavelength of $530nm$ is shown in Figure 5(a). Figure 5(b) illustrates a magnified view of the region of interest (ROI) in Figure 5(a). Figure 5(c) and 5(d) show the same ROI imaged with a conventional $10 \times (NA = 0.24)$ and $20 \times (NA = 0.4)$ objective reflective microscope under the halogen light source respectively for comparison. As seen in Figure 5(b) and 5(d), it is clearly that the image quality of our prototype is comparable to the $20 \times (NA = 0.4)$ objective microscope, but the FOV is ~ 40 times larger than the traditional microscope. It should be noted that we have to use the reflecting optical microscope because of the tissue specimen have adhered

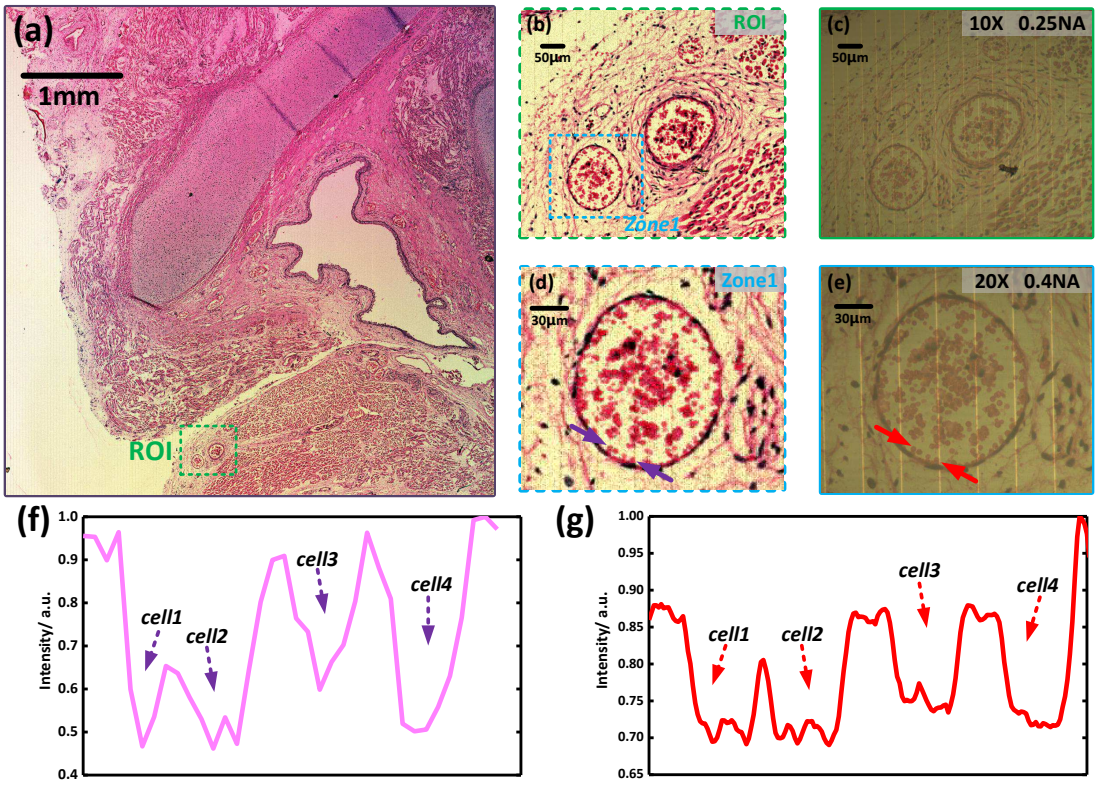

Figure 6. The digitally combined color imaging results of the tissue specimens under the three-color sequential illumination. (a) The color image of the tissue specimens obtained by our RELCSIM system. (b) The enlargement of the green dashed boxed areas of (a). (c) The image with $10\times$ objective reflective microscope corresponding to the green dashed boxed areas of (a). (d) The enlargements of the blue dashed boxed areas of (b). (e) The image with $20\times$ objective reflective microscope corresponding to the blue dashed boxed areas of (b). (f) The line profile along the purple arrows in the (d). (g) The line profile along the red arrows in the (e).

to the chip surface, which is different from the transparent microslide. Therefore the images of the tissue sections obtained by the microscope have a background interference of the metal wire underneath the transparent passivation layer of the chip, as seen the longitudinal white line in Figure 5(b) and 5(c).

Then, we demonstrate the color imaging results of the muscle tissue specimen by the RELCSIM system, as shown in Figure 6(a). Figure 6(b) and 6(c) show the region of the green dashed box in Figure 6(a) obtained by our system and the $10\times(NA=0.24)$ objective microscope respectively. It is obviously that the results of our RELCSIM system have a better image quality. Figure 6(d) is the enlargement of the blue dashed boxed areas of Figure 6(b). We can see that the proposed system can achieve comparable results to the $20\times$ $(NA=0.4)$ objective microscope shown in Figure 6(e). Figure 6(f) and 6(g) show the line profiles along the arrows in Figure 6(d) and 6(e), respectively. Whether in Figure 6(f) or 6(g), the recessed parts of the curve clearly demonstrate the existence of four cells.

From the experimental results above, our RELCSIM system shows its great potential for applications in pathology diagnosis. Benefiting from the submicron resolution and centimeter-level field-of-view, the diagnosis efficiency could be greatly promoted. Compared with the conventional microscope that obtain the full FOV of the tissue specimens by using mechanical scanning, the RELCSIM system is low-cost, compact and portable.

5. Conclusion

We have introduced monochrome and color lensless shadow imaging microscopy based on our large scale submicron-pixel imaging chip to realize the $\sim 1um$ half-pitch resolution and the $\sim 25mm^2$ FOV at the same time. The verification experiments show that the lateral resolution of our system reaches $\sim 1um$, but the longitudinal resolution is slightly less than $1um$. The proposed system achieves comparable performance compared to the traditional $20\times$ objective reflecting microscope, albeit with much larger FOV. The proposed system promises to greatly

improve the efficiency of pathology diagnosis. In the future, we will further reduce the physical size of the pixels and increase the pixel-count in the meantime for higher resolution and larger FOV. In addition, we will also optimize the readout circuits to speed up the framerate for dynamic microscopy.

6. Acknowledgments

This work was financially supported by National Key R&D Program of China (2016YFA0202102), Scientific Research Foundation of Graduate School of Nanjing University (2017ZDL03), Nanjing University Innovation and Creative Program for PhD candidate (2016016), and National Nature Science Foundation Program of China (61571376 and 11304152).

References

[1] J. C. Ahn, C. R. Moon, B. Kim, and K. Lee. Advanced image sensor technology for pixel scaling down toward 1.0m (invited). In *Electron Devices Meeting, 2008. IEDM 2008. IEEE International*, pages 1–4, 2008.

[2] X. Cui, L. M. Lee, X. Heng, W. Zhong, P. W. Sternberg, D. Psaltis, and C. Yang. Lensless high-resolution on-chip optofluidic microscopes for caenorhabditis elegans and cell imaging. *Proceedings of the National Academy of Sciences*, 105(31):10670–10675, 2008.

[3] Z. Grcs and A. Ozcan. On-chip biomedical imaging. *IEEE Reviews in Biomedical Engineering*, 6:29–46, 2013.

[4] S. Isikman, S. S. S. Seo, I. Sencan, A. Erlinger, and A. Ozcan. Lensfree cell holography on a chip: From holographic cell signatures to microscopic reconstruction. pages 404–405, 2009.

[5] C. Kuang, X. Hao, X. Liu, and Y. Li. Evanescent-wave-induced frequency shift for optical superresolution imaging. *Optics Letters*, 38(14):2455, 2013.

[6] D. Lange, C. W. Storment, C. A. Conley, and G. T. A. Kovacs. A microfluidic shadow imaging system for the study of the nematode caenorhabditis elegans in space. *Sensors and Actuators B: Chemical*, 107(2):904–914, 2005.

[7] S. A. Lee, R. Leitao, G. Zheng, S. Yang, A. Rodriguez, and C. Yang. Color capable sub-pixel resolving optofluidic microscope and its application to blood cell imaging for malaria diagnosis. *Plos One*, 6(10):e26127, 2011.

[8] S. A. Lee and C. Yang. A smartphone-based chip-scale microscope using ambient illumination. *Lab on A Chip*, 14(16):3056–3063, 2014.

[9] S. A. Lee, G. Zheng, S. Yang, and C. Yang. Color-capable sub-pixel resolving optofluidic microscope for on-chip cell imaging. *Lab on A Chip*, 10(22):3125–3129, 2010.

[10] A. W. Lohmann, R. G. Dorsch, D. Mendlovic, C. Ferreira, and Z. Zalevsky. Spacebandwidth product of optical signals and systems. *Journal of the Optical Society of America A*, 13(3):470–473, 1996.

[11] A. Ozcan and U. Demirci. Ultra wide-field lens-free monitoring of cells on-chip. *Lab on A Chip*, 8(1):98–106, 2008.

[12] A. Ozcan and E. Mcleod. Lensless imaging and sensing. *Annual Review of Biomedical Engineering*, 18(1):77, 2016.

[13] S. Pang, X. Cui, J. Demodena, Y. M. Wang, P. Sternberg, and C. Yang. Implementation of a color-capable optofluidic microscope on a rgb cmos color sensor chip substrate. *Lab on A Chip*, 10(4):411, 2010.

[14] B. Potsaid, Y. Bellouard, and J. T. Wen. Adaptive scanning optical microscope (asom): A multidisciplinary optical microscope design for large field of view and high resolution imaging. *Opt. Express*, 13(17):6504–6518, 2005.

[15] J. A. Seibert, J. M. Boone, and K. K. Lindfors. Flat-field correction technique for digital detectors. In *Medical Imaging*, pages 348–354, 1998.

[16] H. Xin, D. Erickson, L. R. Baugh, Z. Yaqoob, P. W. Sternberg, D. Psaltis, and C. Yang. Optofluidic microscopya method for implementing a high resolution optical microscope on a chip. *Lab on A Chip*, 6(10):1274, 2006.

[17] G. Zheng, S. A. Lee, S. Yang, and C. Yang. Sub-pixel resolving optofluidic microscope for on-chip cell imaging. *Lab Chip*, 10:3125–3129, 2010.